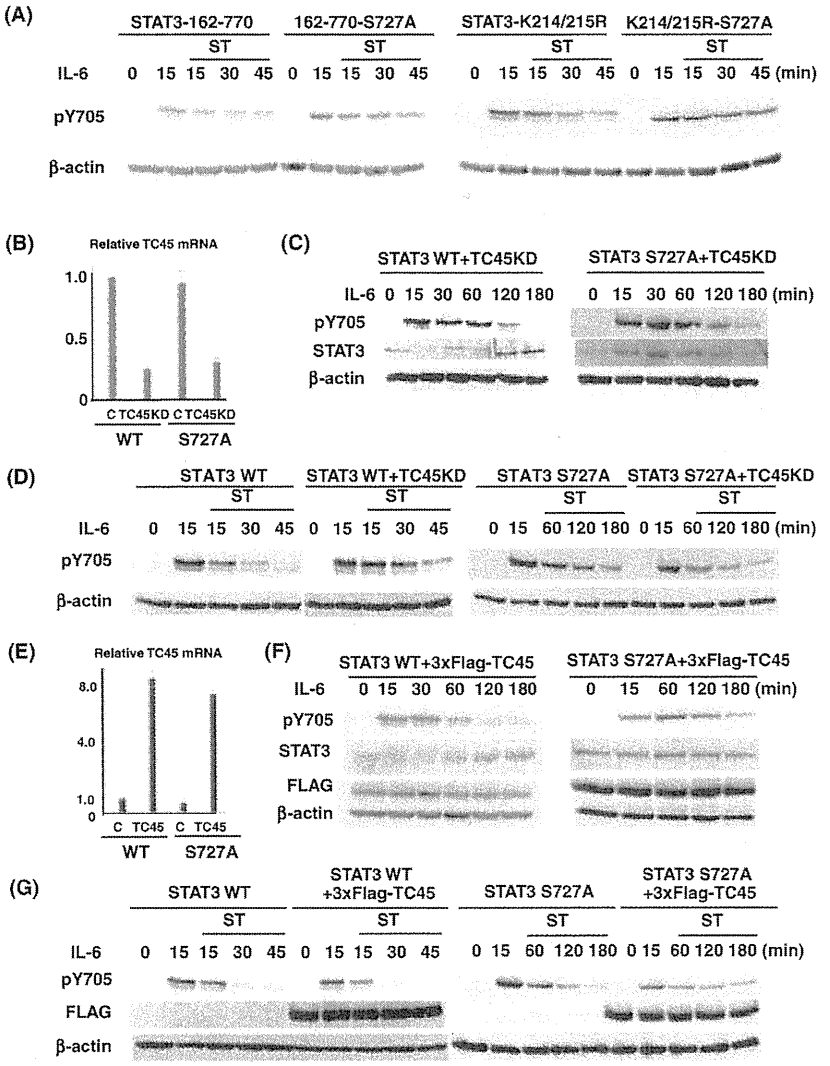

Figure 4 Phospho-Ser727-dependent decrease in pY705 is largely mediated by TC45. (A) HepG2-STAT3-162-770 and HepG2-STAT3-K214/215R cells, both of which are defective for nuclear translocation, were stimulated as in Fig. 3B. Immunoblot analysis was carried out on whole-cell extracts (30 μg per lane) using pY705 and beta-actin antibody as a control. (B) TC45 was knocked down (KD) in HepG2-STAT3WT and HepG2-STAT3S727A cells using a lentivirus for TC45 shRNA. The TC45 mRNA expression levels were measured by qRT-PCR. The level of GAPDH mRNA was used for normalization. The remaining TC45 mRNA levels in TC45-knockdown cells were approximately 25% of controls. (C) HepG2-STAT3WT-TC45KD (STAT3WT+TC45KD: left panel) and HepG2-STAT3 S727A-TC45KD (STAT3S727A+TC45KD: right panel) cells were stimulated with IL-6 for the indicated times. Immunoblotting was carried out on whole-cell extracts (30 μg per lane) using anti-pY705, anti-STAT3, and anti-β-actin. (D) HepG2-STAT3WT and STAT3WT-TC45KD (left panel), HepG2-STAT3S727A and STAT3S727A-TC45KD (right panel) cells were stimulated with IL-6 at 20 ng/mL for 15 min, treated with staurosporine (0.5 μM), and then left for the indicated times. pY705 levels were monitored by immunoblotting. It should be noted that incubation times of STAT3S727A mutant cells were longer than those of STAT3WT cells. (E) HepG2-STAT3WT and STAT3S727A cells were infected with lentivirus for TC45 expression. The TC45 mRNA expression levels in total RNA from each sample were measured by qRT-PCR. The level of GAPDH mRNA was used for normalization. (F) TC45-overexpressed HepG2-STAT3WT (STAT3WT+3×Flag-TC45: left panel) and TC45-overexpressed HepG2-STAT3S727A (STAT3S727A+3×Flag-TC45: right panel) cells were stimulated with IL-6 for the indicated times. Western blotting was carried out on whole-cell extracts (30 μg per lane) using anti-pY705, anti-STAT3, anti-FLAG, and anti-β-actin Abs. (G) HepG2-STAT3WT and HepG2-STAT3WT-3xFlag-TC45 (STAT3WT+3×Flag-TC45) (left panel) and HepG2-STAT3S727A and HepG2-STAT3S727A-3×Flag-TC45 (STAT3S727A+3× FLAG-TC45) (right panel) cells were treated as in (D). Western blotting was carried out on whole-cell extracts (30 μg per lane) using anti-pY705, anti-FLAG, and anti-β-actin Abs. The data representative from two or three independent experiments with similar results are shown for this figure.

© 2012 The Authors
Journal compilation © 2012 by the Molecular Biology Society of Japan/Blackwell Publishing Ltd.

through the TAK1-NLK kinase pathway involving STAT3 as a scaffold (Kojima *et al.* 2005), although the levels of pY705 were much lower and rapidly decreased in both STAT3WT and STAT3S727A under stimulation with G108YRHQ.

To understand the role of phosphorylation at Ser727, we examined the effects of phosphorylation at Ser727 itself in addition to the mutants shown above. We previously showed that the pretreatment of HepG2 with a protein kinase inhibitor H7 and a MEK inhibitor PD98059 greatly inhibited the IL-6-induced Ser727 phosphorylation of STAT3 as well as its accompanying mobility shifts (Abe *et al.* 2001). To test whether Ser727 phosphorylation with mobility shifts is involved in the rapid dephosphory lation of pY705 in STAT3WT, we examined the dephosphorylation of pY705 in the presence of H7 and PD98059. As shown in Fig. 3D, IL-6 rapidly caused tyrosine phosphorylation at Y705 and an increase in the level of pS727 together with apparent mobility shifts of STAT3WT at 15 min. Transient activation of ERK1/2 was detected with anti-phosphoERK at 15 min. Pretreatment with H7 plus PD98059 mostly inhibited both the increases in Ser727 phosphorylation and the mobility shifts. This treatment significantly diminished the rate of pY705 dephosphorylation compared with that in the absence of those inhibitors. The rate of dephosphorylation of pY705 in the presence of H7 plus PD98059 did not match that of STAT3S727A. This difference may result from the incomplete inhibition of S727 phosphorylation with mobility shifts by these inhibitors. Taken together, these data indicate that the phosphorylation of Ser727 is likely to be required for the rapid dephosphorylation of pY705 of STAT3.

Phospho-Ser727-dependent decrease in pY705 is largely mediated by TC45

Next, we searched for the tyrosine phosphatase that is responsible for the phospho-Ser727-dependent dephosphorylation of STAT3 pY705. To date, several PTPs have been reported to act on STAT3. They are SHP1, SHP2, TC45, and PTPRT (ten Hoeve *et al.* 2002; Yamamoto *et al.* 2002; Zhang *et al.* 2007; Kim *et al.* 2010). SHP2 was shown to act on STAT3 by interacting with phosphorylated Y759 in the gp130 YSTV motif. However, the major PTPase(s) sought should act on STAT3 independently of pY759 of gp130, as shown in Fig. 3C, excluding SHP2 as a candidate. Among the above PTPases, only TC45 is localized mainly to the nucleus in HepG2 cells. Then, to get insight into the nature of the candidate PTPase, we first examined where the phosphoSer727-dependent dephosphorylation of pY705 STAT3 occurred—in the cytoplasm or the nucleus. We used two types of STAT3 mutants defective for nuclear translocation, an N-terminal deletion mutant of STAT3-162-770 (Liu *et al.* 2005) and a STAT3-K214/215R mutant (Ma *et al.* 2003). These mutants, with either intact S727 or S727A, were expressed in HepG2-stat3KD cells at comparable levels (data not shown). For each type, STAT3-162-770 or STAT3-K214/215R mutants showed dephosphorylation of pY705 at a significantly slower rate than the dephosphorylation of pY705 of STAT3WT, whereas S727A mutants of both STAT3-162-770 and STAT3-K214/215R showed sustained levels of pY705 as STAT3S727A. These data indicate that in contrast to the STAT3 mutants with S727A, STAT3 with the intact S727 lost phosphorylation at Y705 mainly in the nucleus and to a lesser extent in the cytoplasm. Considering that activated STAT3WT mostly translocates to the nuclei, it is likely that phospho-Ser727-dependent dephosphorylation of pY705 may be mainly regulated in the nucleus. Thus, PTPase in the nucleus is likely to be responsible for the dephosphorylation of pY705 in a phospho-Ser727-dependent manner. However, the possibility of some contribution of phosphatase(s) outside the nucleus should be kept in mind, considering that STAT3 itself may shuttle between cytoplasm and nucleus (Liu *et al.* 2005). Because TC45 was mainly localized to the nucleus in HepG2 cells (data not shown), we examined how much TC45 contributed to the dephosphorylation of STAT3 at Y705 in a phospho-Ser727-dependent manner. To evaluate the role of TC45, we knocked down TC45 in both HepG2-STAT3WT and HepG2-STAT3S727A cells using a lentiviral expression system for TC45 shRNA (Fig. 4B). These cells were stimulated with IL-6 for the indicated times, and the STAT3 Y705 phosphorylation was monitored (Fig. 4C). The TC45 knockdown (TC45KD) extended the duration of the pY705 level in STAT3WT, compared with the results shown in Fig. 2D, whereas TC45KD did not alter the rate of pY705 dephosphorylation in STAT3S727A, indicating that TC45 greatly affected the pY705 level of STAT3 with the intact Ser727. It should be noted that the time points used for STAT3S727A cover a longer time frame than that for STAT3WT. To further test the role of TC45, we overexpressed 3×FLAG-TC45 in HepG2-STAT3WT cells and HepG2-STAT3S727A cells. The expression levels of TC45 were approximately

© 2012 The Authors
Journal compilation © 2012 by the Molecular Biology Society of Japan/Blackwell Publishing Ltd.

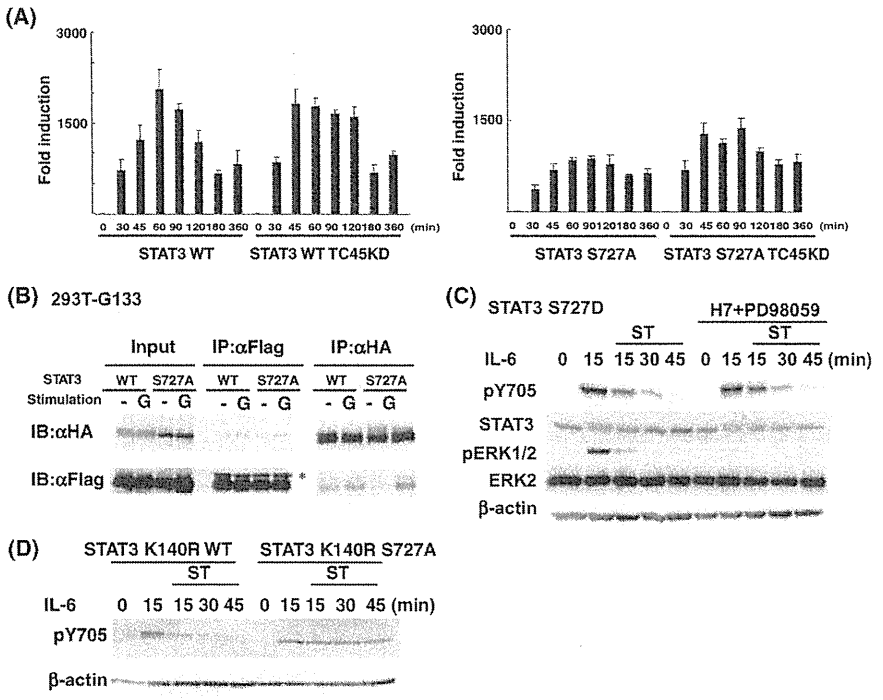

Figure 5 TC45 on STAT3 pY705 needs a post-phospho-Ser727 event(s) to function. (A) HepG2-STAT3WT and HepG2-STAT3WT-TC45KD (left panel), HepG2-STAT3S727A, and HepG2-STAT3S727SA-TC45KD (right panel) cells were stimulated with 20 ng/mL IL-6 for the indicated times. The *socs3* mRNA expression levels in total RNA from each sample were measured by qRT-PCR as in Fig. 1B. The data are averages of three independent experiments; error bars are the standard deviations. (B) 293T-G133 cells were transiently transfected with either HA-tagged STAT3WT or HA-STAT3S727A together with a 3×FLAG-tagged TC45-DA/CS mutant (Asp182 to Ala, Cys216 to Ser). Transfected cells were unstimulated (–) or stimulated with G-CSF at 50 ng/mL for 15 min (G). Whole-cell extracts were immunoprecipitated with anti-FLAG or anti-HA antibodies. Immunoprecipitates were analyzed by immunoblotting using anti-HA and anti-Flag Abs. An asterisk (*) shows a nonspecific protein. (C) HepG2-STAT3S727D cells were pretreated with or without H7 (100 μM) and PD98059 (50 μM) for 30 min then stimulated with IL-6 at 20 ng/mL for 15 min, and treated with staurosporine (ST) (0.5 μM) for the indicated times. Immunoblot analysis was carried out on whole-cell extracts (30 μg per lane) using indicated antibodies. (D) HepG2-STAT3Lys140Arg(K140R)/WT and STAT3K140R/S727A were stimulated with IL-6 (20 ng/mL) for 15 min, and treated with ST (0.5 μM) for the indicated times, then pY705 levels were monitored by immunoblotting.

eight times that of endogenous TC45 mRNA (Fig. 4E). Overexpressed TC45 reduced the overall levels of pY705 of both STAT3WT and STAT3S727A, probably due to the effect on the activity of JAK kinases (Simoncic *et al.* 2002). However, overexpressed TC45 shortened the duration of pY705 of STAT3WT but not that of STAT3S727A (Fig. 4F). This was also the case for the dephosphorylation process analyzed by the use of ST (Fig. 4G). Overexpressed TC45 caused rapid dephosphorylation of pY705 of STAT3WT but did not alter the dephosphorylation rate of pY705 of STAT3S727A. Consistent with this, the inhibition of phospho-Ser727 by the kinase inhibitors, shown in Fig. 3C, also reduced the rate of pY705 dephosphorylation even in the presence of overexpressed TC45 (data not shown).

Unidentified event(s) because of phospho-Ser727 may affect the function of TC45 on STAT3 pY705

To further support the notion that TC45 functions in dephosphorylation of pY705 in a phospho-Ser727-dependent manner, we examined the effect of a TC45 knockdown on STAT3-dependent *socs3* mRNA expression (Fig. 5A). TC45KD caused more sustained *socs3* mRNA expression in STAT3WT cells but not in STAT3S727A cells. Slightly higher *socs3* mRNA expression was observed throughout the tested period in STAT3S727A cells. This may result from the regulation of JAKs activity by TC45 (Simoncic *et al.* 2002). All of the data shown above indicate that TC45 is largely responsible for the dephosphorylation of STAT3 pY705 in a phospho-Ser727-dependent manner.

© 2012 The Authors
Journal compilation © 2012 by the Molecular Biology Society of Japan/Blackwell Publishing Ltd.

We next addressed how phospho-Ser727 of STAT3 affected the function of TC45. We then tested whether phospho-Ser727 was required for the interaction between STAT3 and TC45. For this purpose, we used a TC45 mutant, TC45-DA/CS that lacked the phosphatase activity as often used to see the interaction between certain tyrosine phosphatases and their substrates (Tiganis *et al.* 1999; Tonks *et al.* 2004). We transiently expressed HA-tagged STAT3WT or HA-STAT3S727A together with 3×FLAG-tagged TC45-DA/CS in 293T-G133 cells expressing the GCSF-R-gp130 chimeric receptor containing a truncated gp130 with cytoplasmic 133 amino acid residues with both a YSTV motif and a YRHQ motif, G133 (Abe *et al.* 2001). As shown in Fig. 5B, the anti-FLAG antibody immunoprecipitated TC45-DA/CS together with small amounts of HA-STAT3WT or HA-STAT3S727A even in the absence of receptor stimulation, though gp130 stimulation increased the interaction between TC45 and HA-STAT3WT or HA-STAT3S727A. Consistently, immunoprecipitated complexes of HA-STAT3WT or HA-STAT3S727A contained FLAG-TC45-DA/CS, especially after gp130 stimulation. Thus, TC45 interacts with STAT3 independently of phospho-Ser727, suggesting the presence of unidentified and phospho-Ser727-dependent mechanism(s) that allow TC45 to function well.

To gain insight into the events after Ser727 phosphorylation that affect the TC45 function, we tested whether the kinase activities sensitive to H7+PD98059 play a role in regulating pY705 of STAT3S727D. Pretreatment of HepG2-STAT3S727D with H7+PD98059 did not inhibit the dephosphorylation of pY705 (Fig. 5C). Importantly, the slight changes in STAT3S727D mobility after IL-6 stimulation were observed even in the presence of H7+PD98059 (Fig. 5C). Together with the results shown in Fig. 3D, this result indicates that the kinase activities sensitive to H7+PD98059 in IL-6 signals are involved in Ser727 phosphorylation but not in the post-phospho-Ser727 events causing a further mobility shift nor in enhancing the pY705 dephosphorylation process. In relation to this matter, recently, Yang *et al.* (2010) showed that dimethylation of STAT3 at K140 by SET9 after Ser727 phosphorylation in the nucleus inhibits STAT3 activity by suppressing the level of pY705 of STAT3. Therefore, we tested whether STAT3K140R mutants defective for being methylated might lose the phospho-Ser727-dependent regulation of pY705 in our system. We expressed both STAT3K140R/WT and STAT3K140R/S727A at a comparable level in HepG2-stat3KD cells (data not shown). As shown in Fig. 5D, STAT3K140R/WT showed rapid dephosphorylation of pY705 under the tyrosine-kinase inhibition, whereas STAT3-K140R/S727A showed very slow dephosphorylation of pY705. This result excluded the role of a K140 modification in the phospho-Ser727-dependent pY705 dephosphorylation in our HepG2-STAT3 reconstitution system. These data suggest that phospho-Ser727 is functionally required for the dephosphorylation of pY705 largely by TC45 through possibly recruiting a regulatory molecule(s) targeting to phospho-Ser727 or to another region modified in a phospho-Ser727-dependent manner that is distinct from K140 methylation.

Discussion

In this study, we first showed that the intact Ser727 of STAT3 is required for both the maximal transcription of the *socs3* gene, one of the STAT3 target genes, and the restricted duration of its mRNA expression from the mechanism intrinsic to the state of STAT3. We showed that this regulated duration of STAT3 action at least partly resulted from phosphorylation at Ser727 by using a combination of the HepG2-stat3KD reconstituted with various STAT3 mutants and the kinase inhibitors, H7 and PD98059, that interfere with phosphorylation of Ser727 in IL-6 signals. This dual role for phospho-Ser727 of STAT3 might be physiologically important to give proper responses with regulated strength and duration of STAT3 activity. The effect of phospho-Ser727 of STAT3 on the regulated gene expression was also observed in other STAT3-inducible genes, including *tis11*/TTP and acute phase reactants, *saa1* and *saa2* (unpublished data). ST was used in this study to efficiently inhibit further phosphorylation of Y705 by tyrosine kinases in IL-6/gp130 signals. We should mention the possibility that this reagent might inhibit the kinase activities of some serine/threonine kinases involved in the pathways leading to phospho-Ser727 in this receptor system. However, considering the fact that phospho-Ser727 of STAT3 remained well after the rapid decrease of pY705 in STAT3 WT after the treatment with ST (Fig. 3D), we believe that the role of phospho-Ser727 in the rapid dephosphorylation of Y705 was properly evaluated in this study.

Multiple PTPases including SHP2, SHP1, TC45, and PTP-RT (ten Hoeve *et al.* 2002; Yamamoto *et al.* 2002; Zhang *et al.* 2007; Kim *et al.* 2010) have been shown to regulate STAT3 activity. Among these PTPases, we have shown that TC45 is likely a major PTPase for the phospho-Ser727-dependent pY705

© 2012 The Authors
Journal compilation © 2012 by the Molecular Biology Society of Japan/Blackwell Publishing Ltd.

dephosphorylation from the following layers of supporting evidence: (i) phospho-Ser727-dependent dephosphorylation is likely to occur mainly in the nucleus, as judged by the reduced rate of pY705 dephosphorylation in two STAT3 mutants devoid of nuclear translocation, (ii) TC45-knockdown affected the pY705 duration as well as the duration of *socs3* mRNA expression in HepG2-STAT3WT cells but not in HepG2-STAT3S727A cells, (iii) overexpression of TC45 again affected the pY705 dephosphorylation of STAT3WT but not that of STAT3S727A. However, at least one cytoplasmic or membrane phosphatase distinct from TC45 may need the intact Ser727 or phosphorylated Ser727 to function, based on the results that S727A in the STAT3 mutants devoid of nuclear translocation also showed sustained pY705 (Fig. 4A). Considering that when cells were stimulated with the YXXQ signal alone instead of IL-6, both STAT3WT and STAT3S727A showed a higher dephosphorylation rate (Fig. 3C), there must be another tyrosine phosphatase that dephosphorylates pY705 independently of phospho-Ser727 under the pYXXQ-derived signals. Thus, STAT3 inactivation through tyrosine dephosphorylation is regulated by multiple mechanisms involving multiple PTPases and multiple signals.

Interestingly, the interaction of TC45 with STAT3 did not require phospho-Ser727. This suggests that the action of TC45 on pY705 of STAT3 is regulated not only by the interaction between them but also by some unidentified mechanism(s) that occurs in a phospho-Ser727-dependent manner. Such mechanisms seem to use a regulatory molecule(s) targeting a region including phospho-Ser727 or another STAT3 region modified in a phospho-Ser727-dependent manner. The possible STAT3 modifications involved in such regulation may include phosphorylation, acetylation, methylation, sumoylation, ubiquitilation, and other unidentified modifications. Yang *et al.* (2010) recently showed that activated STAT3 was methylated on K140 by the histone methyltransferase SET9 in the nucleus after Ser727 phosphorylation and that the methylation of STAT3 had negative regulatory effects on pY705 and STAT3-dependent transcription of some genes, including the *socs3* gene. However, we found that STAT3-K140 methylation did not account for the phospho-Ser727-dependent dephosphorylation of Y705 in our system. STAT3 has been shown to be acetylated at K685 (Wang *et al.* 2005; Yuan *et al.* 2005), K49 and K87 (Ray *et al.* 2005), and K679, K685, K707, and K709 (Nie *et al.* 2009). There was one report showing a relationship between STAT3 acetylation and phosphotyrosine levels. Nie *et al.* (2009) showed that SirT1 negatively regulates STAT3 phosphotyrosine level by deacetylating the multiply acetylated STAT3. Based on their data, it is likely that acetylation of STAT3 at multiple lysines in the carboxy-terminus, K679, K685, K707, and K709, protects activated STAT3 from PTPase action. Thus, such acetylation of STAT3 causes sustained activation of STAT3, making it unlikely for the acetylation of STAT3 on these sites to be involved in the negative regulation shown in this study. We have seen mobility shifts of STAT3WT but not of STAT3S727A after IL-6 stimulation or stimulation of gp130-YXXQ-derived signals, as shown in Fig. 3A,C,D. These mobility shifts most likely result from phosphorylation of multiple sites in addition to Ser727. As the STAT3S727A mutant does not show apparent mobility shifts, such phosphorylation events, if any, should be dependent on phospho-Ser727. This is also supported by the result showing that STAT3S727D itself caused a slight mobility shift but that STAT3S727D showed a further small mobility shift after stimulation (Fig. 5C). Because the contribution of pY705 in the mobility shifts seemed to be negligible, as shown Fig. 3A, in addition to the phosphorylation of Y705, STAT3S727D is likely to undergo a further modification that results in the further mobility shift. Interestingly, the modification event observed in IL-6-stimulated STAT3S727D was resistant to the treatment with H7+PD98059. Considering that dephosphorylation of pY705 of STAT3S727D is also resistant to the kinase inhibitors, the unidentified events affecting the mobility shift because of phospho-Ser727, or S727D, might be involved in regulating the activity of PTPases including TC45. Identification of modification event(s) and the amino acid residues receiving such modification is needed to clarify the mechanism.

The roles of phospho-Ser727 of STAT3 in the gene transcription have been reported since the discovery of the phosphorylation of Ser727, in addition to the critical tyrosine phosphorylation (Wen *et al.* 1995). Most studies relied on the use of the STAT3 mutants, STAT3S727A and STAT3S727D (Wen & Darnell 1997; Abe *et al.* 2001; Shen *et al.* 2004), used in this study. The use of such mutants may reduce the validity of deductions about the role of phospho-Ser727 in some cases. Sun *et al.* (2006) showed that the conserved LPMSP motif around Ser727 itself is required for p300 recruitment by STAT3 to the target gene regulatory regions. They showed that some mutations introduced at the motif disrupt the proper

© 2012 The Authors
Journal compilation © 2012 by the Molecular Biology Society of Japan/Blackwell Publishing Ltd.

recruitment of p300 without hampering the phosphorylation of Ser727, although their findings do not exclude the role of phospho-Ser727 in the regulation of STAT3-dependent gene transcription. In our preliminary experiments, HepG2-STAT3S727D cells induced a *socs3* mRNA expression of short duration, consistent with the role of phospho-Ser727 in enhancing dephosphorylation of pY705 (unpublished data). Studies of the regulatory mechanisms by which IL-6 activates transcription of STAT3 target genes, including the roles of phospho-Ser727, are currently underway. The study of the role of phospho-Ser727 of STAT3 in gene regulation apparently requires more sophisticated methods.

Although we report that the role of phospho-Ser727 in IL-6 signals negatively regulates the duration of STAT3 activity by enhancing dephosphorylation of pY705 largely through TC45, the same mechanism may inhibit STAT3 activity when phosphorylation of Ser727 precedes Y705 tyrosine phosphorylation in the cases of the combined stimulation of cells with some factors causing phospho-Ser727 and some causing pY705 of STAT3, or under some conditions in which cells have both active serine/threonine kinases for Ser727 and tyrosine kinases for Tyr705 of STAT3. Actually, such cases or conditions have been reported. Andersson *et al.* (2007) showed that insulin inhibits IL-6-induced STAT3 activity through SHP-2 and MEK/ERK1/2-dependent pathways. They showed that insulin enhanced phospho-Ser727 but reduced phospho-Tyr705 of STAT3 when given together with IL-6 and that the inhibitory effect of insulin was mostly reversed with PD98059 treatment. Shi *et al.* (2006) found that the enhanced level of STAT3 Ser727 phosphorylation during mitosis, which was shown to be induced by cyclin-dependent kinase 1, correlated well with a reduction of Y705 phosphorylation of STAT3 and that the reduction of STAT3 activity during mitosis was likely to be involved in the regulation of the cell cycle. These two reports discussed the negative relationship between phospho-Ser727 and phospho-Tyr705 of STAT3. Our findings on the role of phosphorylation of Ser727 in negatively regulating pY705 largely through TC45 may explain the underlying mechanism of their results.

STAT3 activation has been shown to be critical in the development of certain types of tumors (Bowman *et al.* 2000; Kim *et al.* 2007). In the many instances of such *in vivo* tumor cells, both phospho-Y705 and phospho-S727 have been often observed. In those cells, phospho-S727 in STAT3 has been argued to have positive roles in STAT3 function (Lee *et al.* 2009). It is possible that some mechanisms negating the negative role of phospho-Ser727 may be present in some tumor cells utilizing STAT3 as a transcription factor causing survival and proliferative signals.

Our study provides evidence showing that phospho-Ser727 enhances dephosphorylation of pY705 of STAT3 largely through TC45, and implies the existence of an unidentified post-phospho-Ser727 process for the efficient function of TC45. Thus, in-depth understanding of the molecular mechanisms following phospho-Ser727 will shed light on the mechanisms determining the overall roles of phospho-Ser727, both negative and positive, in STAT3 functions in different settings.

Experimental procedures

Reagents and antibodies

Recombinant human IL-6 was a gift from Ajinomoto Research Institute (Tokyo, Japan). Recombinant human G-CSF was purchased from Kyowa Hakko Kirin Co., Ltd. (Tokyo, Japan). Antibodies (Abs) to STAT3, RNA polymerase II (Pol II), β-actin, ERK1/2, and phospho-ERK1/2 were from Santa Cruz Biotechnology (Santa Cruz, CA, USA). Abs to phospho-STAT3 (Tyr705) and phospho-STAT3 (Ser727) were from Cell Signaling Technology (Beverly, MA, USA). The anti-FLAG monoclonal Ab (M2) was from Sigma-Aldrich (Saint Louis, MO, USA), and anti-HA Ab was from Roche Diagnostics (Indianapolis, IN, USA). 1-(5-Iso-quinolinylsulfonyl)-2-methylpiperazine (H7) was from Sigma-Aldrich. MEK inhibitor PD98059 was from Calbiochem (La Jolla, CA, USA). All other reagents purchased from Nacalai Tesque Inc. (Kyoto, Japan).

Plasmids and siRNA

The siRNA-resistant STAT3WT was described previously (Zhao *et al.* 2004). All of the STAT3 mutants, STAT3S727A (Ser727 to Ala), STAT3S727D (Ser727 to Asp), STAT3K214R/K215R/WT (Lys214 to Arg, Lys215 to Arg), STAT3K214R/K215R/S727A, STAT3K140R/WT (Lys140 to Arg), and STAT3K140R/S727A were made using the quick-change mutation system (Stratagene, La Jolla, CA, USA). Two STAT3 N-terminal deletion mutants, STAT3-162-770/WT and STAT3-162-770/S727A, were produced by PCR. Sequences of all of the mutants were verified by DNA sequencing. Each Stat3 cDNA was transferred into a lentiviral vector, pCSII-EF-MCS-IRES-Venus (a gift from H. Miyoshi, RIKEN, Tsukuba, Japan). To generate the pCSII-EF-3×FlagTC45, the entire coding region was amplified by PCR using pCMV-SPORT6-TC45 (Clone ID 3872164) purchased from OpenBiosytems (Huntsville, AL, USA) as a template and the resulting cDNA with the *Eco*RI and *Bam*HI

© 2012 The Authors
Journal compilation © 2012 by the Molecular Biology Society of Japan/Blackwell Publishing Ltd.

sites at both ends was cloned into pCSII-EF-3xFLAG-IRES-Venus at the *Eco*RI/*Bam*HI site. The TC45DA/CS (Asp182 to Ala, Cys216 to Ser) mutant was made using the quick-change mutation system. To make TC45 knockdown cells, we used a lentiviral miRNA-type shRNA expression system. The oligonucleotide for the shRNA against human TC45 was as follows: TC45-mishRNA-1077: TGCTGAAAGGCAGGAGA TAAGTCTTCGTTTTGGCCACTGACTGACGAAGACTT CTCCTGCCTTT.

Cell lines

All HepG2 cell lines were grown in DMEM supplemented with 10% FCS (GIBCO, Grand Island, NY, USA), and HEK293T cells were grown with 5% FCS. The HepG2 cell line with stat3 mRNA knockdown (HepG2-stat3KD) was used for reconstitution of mutated STAT3 (Zhao *et al.* 2004). Lentiviral preparations expressing STAT3 mutants were produced as described previously and infected into HepG2-stat3KD cells.

Immunoblotting and immunoprecipitation

The cells were washed twice with ice-cold phosphate-buffered saline and then lysed with whole-cell extract buffer (20 mM Hepes, pH 7.9, 1% NP-40, 400 mM NaCl, 20% glycerol, 10 mM NaF, 1 mM PMSF, 1 mM sodium vanadate, 1 mM EDTA, 1 mM EGTA, 1 μg/mL leupeptin, 1 μg/mL pepstatin, and 1 μg/mL aprotinin). The cell lysates were centrifuged at 14 000 *g* for 10 min at 4 °C, and the resulting supernatants were used. Immunoprecipitation analysis was carried out as described previously (Kojima *et al.* 2005). Whole cell extracts or immunoprecipitates were separated by 7.5% SDS–PAGE, transferred onto polyvinylidene difluoride (PVDF) membranes, and probed with the indicated antibodies. Signals were detected with Chemi-Lumi One (Nacalai Tesque).

Quantitative real-time PCR

RNA was isolated with Sepasol RNA I super (Nacalai Tesque) and treated with RQ1 RNase-free DNase I (Promega, Madison, WI, USA). Reverse transcriptase reaction for cDNA synthesis was made using a ReverTra Ace qPCR RT kit (Toyobo Co Ltd., Osaka, Japan). Relative quantification was carried out using the ABI 7500 Fast System (Applied Biosystems). Primers were designed using PRIMER EXPRESS software (Applied Biosystems), and sequences are as below. Relative quantities of target transcripts were calculated from duplicate samples after normalization of the data against the endogenous control, hGAPDH-Forward; 5′-GCACCGTCAA GGCTGAGAAC-3′, hGAPDH-Reverse; 5′-TGGTGAAGAC GCCAGTGGA-3′, hSOCS3-Forward; 5′-GGAATGTAGCA GCGATGGAA-3′, hSOCS3-Reverse; 5′-GCCCTGTCCAGC CCAATAC-3′, hGCSFRgp108YRHQ-Forward; 5′-CTCTCC TGCCTCATGAACCTC-3′, hGCSFRgp108YRHQ-Reverse; 5′-GTGAAGCTGGTGGGTAGGTG-3′, hSTAT3-Forward; 5′-ACTCCATCCTGGGCGACAGT-3′, hSTAT3-Reverse; 5′-TTGACCTGAAGCCCGTTTC-3′, hTC45-Forward; 5′-TT TTGGAGTCCCTGAATCACC-3′, hTC45-Reverse; 5′-GCC CAATGCCTGCACTACA-3′.

Chromatin immunoprecipitation assays

Chromatin immunoprecipitation (ChIP) was carried out according to the manufacturer's instructions (Upstate Biotechnology, Lake Placid, NY, USA). Briefly, the HepG2-derivative cell lines were stimulated with IL-6 at 20 ng/mL for the indicated times, and the cells were fixed with 1% formaldehyde (final concentration) for 10 min at 37 °C, lysed, and sonicated. Immunoprecipitates with specific antibodies were incubated with proteinase K overnight at 65 °C, and then the DNA fragments included in the immunoprecipitates were purified. PCR was carried out using the ABI 7500 Fast System (Applied Biosystems, Foster City, CA, USA). The primer sets were the following: the human SOCS3 promoter region (−115 to −49), Forward 5′-TTTCTCTGCTGCGAG TAGTGACTAA-3′, Reverse 5′-CCCCCGATTCCTGGA ACT-3′ and the 3′ end of the SOCS3 gene (2899 to 3024), Forward 5′-GGAATGTAGCAGCGATGGAA-3′, Reverse 5′-GCCCTGTCCAGCCCAATAC-3′.

Acknowledgements

We thank J. Kanbara for her technical support, and Hiroyuki Miyoshi for the lentiviral vector system. Lentivirus particles were prepared in the Central Laboratory of Osaka City University. This work was supported in part by the Ministry of Education, Culture, Sports, Science and Technology of Japan; Otsuka Pharmaceutical Co. Ltd., and the Osaka Foundation for the Promotion of Clinical Immunology.

References

Abe, K., Hirai, M., Mizuno, K., Higashi, N., Sekimoto, T., Miki, T., Hirano, T. & Nakajima, K. (2001) The YXXQ motif in gp130 is crucial for STAT3 phosphorylation at Ser727 through an H7-sensitive kinase pathway. *Oncogene* **20**, 3464–3474.

Andersson, C.X., Sopasakis, V.R., Wallerstedt, E. & Smith, U. (2007) Insulin antagonizes interleukin-6 signaling and is anti-inflammatory in 3T3-L1 adipocytes. *J. Biol. Chem.* **282**, 9430–9435.

Boulton, T.G., Zhong, Z., Wen, Z., Darnell, J.E., Stahl, N. & Yancopoulos, G.D. (1995) STAT3 activation by cytokines utilizing gp130 and related transducers involves a secondary modification requiring an H7-sensitive kinase. *Proc. Natl Acad. Sci. USA* **92**, 6915–6919.

Bowman, T., Garcia, R., Turkson, J. & Jove, R. (2000) STATs in oncogenesis. *Oncogene* **19**, 2474–2488.

Chung, J., Uchida, E., Grammer, T.C. & Blenis, J. (1997) STAT3 serine phosphorylation by ERK-dependent and

© 2012 The Authors
Journal compilation © 2012 by the Molecular Biology Society of Japan/Blackwell Publishing Ltd.

-independent pathways negatively modulates its tyrosine phosphorylation. *Mol. Cell. Biol.* **17**, 6508–6516.

Darnell, J.E. Jr (1997) STATs and gene regulation. *Science* **277**, 1630–1635.

Darnell, J.E. Jr, Kerr, I.M. & Stark, G.R. (1994) Jak-STAT pathways and transcriptional activation in response to IFNs and other extracellular signaling proteins. *Science* **264**, 1415–1421.

Decker, T. & Kovarik, P. (2000) Serine phosphorylation of STATs. *Oncogene* **19**, 2628–2637.

Fu, A.K., Fu, W.Y., Ng, A.K., Chien, W.W., Ng, Y.P., Wang, J.H. & Ip, N.Y. (2004) Cyclin-dependent kinase 5 phosphorylates signal transducer and activator of transcription 3 and regulates its transcriptional activity. *Proc. Natl Acad. Sci. USA* **101**, 6728–6733.

Fukada, T., Hibi, M., Yamanaka, Y., Takahashi-Tezuka, M., Fujitani, Y., Yamaguchi, T., Nakajima, K. & Hirano, T. (1996) Two signals are necessary foe cell proliferation induced by a cytokine receptor gp130: involvement of STAT3 in anti-apoptosis. *Immunity* **5**, 449–460.

Haspel, R.L. & Darnell, J.E. (1999) A nuclear protein tyrosine phosphatase is required for the inactivation of Stat1. *Proc. Natl Acad. Sci. USA* **96**, 10188–10193.

Hirano, T., Nakajima, K. & Hibi, M. (1999) Signaling mechanisms through gp130: a model of the cytokine system. *Cytokine Growth Factor Rev.* **8**, 241–252.

ten Hoeve, J., de Jesus Ibarra-Sanchez, M., Fu, Y., Zhu, W., Tremblay, M., David, M. & Shuai, K. (2002) Identification of a nuclear Stat1 protein tyrosine phosphatase. *Mol. Cell. Biol.* **22**, 5662–5668.

Jain, N., Zhang, T., Kee, W.H., Li, W. & Cao, X. (1999) Protein kinase C delta associates with and phosphorylates Stat3 in an interleukin-6-dependent manner. *J. Biol. Chem.* **274**, 24392–24400.

Kim, D.J., Chan, K.S., Sano, S. & DiGiovanni, J. (2007) Signal transducer and activator of transcription 3 (Stat3) in epithelial carcinogenesis. *Mol. Carcinog.* **46**, 725–731.

Kim, D.J., Tremblay, M.L. & DiGiovanni, J. (2010) Protein tyrosine phosphatases, TC-PTP, SHP1, and SHP2, cooperate in rapid dephosphorylation of Stat3 in keratinocytes following UVB irradiation. *PLoS ONE* **5**, e10290.

Kojima, H., Sasaki, T., Ishitani, T., Iemura, S., Zhao, H., Kaneko, S., Kunimoto, H., Natsume, T., Matsumoto, K. & Nakajima, K. (2005) STAT3 regulates Nemo-like kinase by mediating its interaction with IL-6-stimulated TGFbeta-activated kinase 1 for STAT3 Ser-727 phosphorylation. *Proc. Natl Acad. Sci. USA* **102**, 4524–4529.

Lee, H., Herrmann, A., Deng, J.H., Kujawski, M., Niu, G., Li, Z., Forman, S., Jove, R., Pardoll, D.M. & Yu, H. (2009) Persistently activated Stat3 maintains constitutive NF-kappaB activity in tumors. *Cancer Cell* **15**, 283–293.

Lehmann, U., Schmitz, J., Weissenbach, M., Sobota, R.M., Hortner, M., Friederichs, K., Behrmann, I., Tsiaris, W., Sasaki, A., Schneider-Mergener, J., Yoshimura, A., Neel, B.G., Heinrich, P.C. & Schaper, F. (2003) SHP2 and SOCS3 contribute to Tyr-759-dependent attenuation of interleukin-6 signaling through gp130. *J. Biol. Chem.* **278**, 661–671.

Levy, D.E. & Darnell, J.E. (2002) Stats: transcriptional control and biological impact. *Nat. Rev. Mol. Cell Biol.* **3**, 651–662.

Li, W., Nishimura, R., Kashishian, A., Batzer, A.G., Kim, W.J.H., Cooper, J.A. & Schlessinger, J. (1994) A new function for a phosphotyrosine phosphatase: linking GRB2-Sos to a receptor tyrosine kinase. *Mol. Cell. Biol.* **14**, 509–517.

Liu, L., McBride, K.M. & Reich, N.C. (2005) STAT3 nuclear import is independent of tyrosine phosphorylation and mediated by importin-alpha3. *Proc. Natl Acad. Sci. USA* **102**, 8150–8155.

Lufei, C., Koh, T.H., Uchida, T. & Cao, X. (2007) Pin1 is required for the Ser727 phosphorylation-dependent Stat3 activity. *Oncogene* **26**, 7656–7664.

Ma, J., Zhang, T., Novotny-Diermayr, V., Tan, A.L.C. & Cao, X. (2003) A novel sequence in the coiled-coil domain of Stat3 essential for its nuclear translocation. *J. Biol. Chem.* **278**, 29252–29260.

Mertens, C. & Darnell, J.E. (2007) SnapShot: JAK-STAT signaling. *Cell* **131**, 612.

Nicholson, S.E., Willson, T.A., Farley, A., Starr, R., Zhang, J.G., Baca, M., Alexander, W.S., Metcalf, D., Hilton, D.J. & Nicola, N.A. (1999) Mutational analyses of the SOCS proteins suggest a dual domain requirement but distinct mechanisms for inhibition of LIF and IL-6 signal transduction. *EMBO J.* **18**, 375–385.

Nie, Y., Erion, D.M., Yuan, Z., Dietrich, M., Shulman, G.I., Horvath, T.L. & Gao, Q. (2009) STAT3 inhibition of gluconeogenesis is downregulated by SirT1. *Nat. Cell Biol.* **11**, 492–500.

Ohkawara, B., Shirakabe, K., Hyodo-Miura, J., Matsuo, R., Ueno, N., Matsumoto, K. & Shibuya, H. (2004) Role of the TAK1-NLK-STAT3 pathway in TGF-beta-mediated mesoderm induction. *Genes Dev.* **18**, 381–386.

Ray, S., Boldogh, I. & Brasier, A.R. (2005) STAT3 NH2-terminal acetylation is activated by the hepatic acute-phase response and required for IL-6 induction of angiotensinogen. *Gastroenterology* **129**, 1616–1632.

Sato, N., Kawai, T., Sugiyama, K., Muromoto, R., Imoto, S., Sekine, Y., Ishida, M., Akira, S. & Matsuda, T. (2005) Physical and functional interactions between STAT3 and ZIP kinase. *Int. Immunol.* **17**, 1543–1552.

Schmitz, J., Dahmen, H., Grimm, C., Gendo, C., Müller-Newen, G., Heinrich, P.C. & Schaper, F. (2000) The cytoplasmic tyrosine motifs in full-length glycoprotein 130 have different roles in IL-6 signal transduction. *J. Immunol.* **164**, 848–854.

Schuringa, J.J., Schepers, H., Vellenga, E. & Kruijer, W. (2001) Ser727-dependent transcriptional activation by association of p300 with STAT3 upon IL-6 stimulation. *FEBS Lett.* **495**, 71–76.

Shen, Y., Schlessinger, K., Zhu, X., Meffre, E., Quimby, F., Levy, D.E. & Darnell, J.E.. Jr (2004) Essential role of STAT3 in postnatal survival and growth revealed by mice

© 2012 The Authors
Journal compilation © 2012 by the Molecular Biology Society of Japan/Blackwell Publishing Ltd.

lacking STAT3 serine 727 phosphorylation. *Mol. Cell. Biol.* **24**, 407–419.

Shi, X., Zhang, H., Paddon, H., Lee, G., Cao, X. & Pelech, S. (2006) Phosphorylation of STAT3 serine-727 by cyclin-dependent kinase 1 is critical for nocodazole-induced mitotic arrest. *Biochemistry* **45**, 5857–5867.

Simoncic, P.D., Lee-Loy, A., Barber, D.L., Tremblay, M.L. & McGlade, C.J. (2002) The T cell protein tyrosine phosphatase is a negative regulator of janus family kinases 1 and 3. *Curr. Biol.* **12**, 446–453.

Stahl, N., Farruggella, T.J., Boulton, T.G., Zhong, Z., Darnell, J.E. Jr & Yancopoulos, G.D. (1995) Choice of STATs and other substrates specified by modular tyrosine-based motifs in cytokine receptors. *Science* **267**, 1349–1352.

Sun, W., Snyder, M., Levy, D.E. & Zhang, J.J. (2006) Regulation of Stat3 transcriptional activity by the conserved LPMSP motif for OSM and IL-6 signaling. *FEBS Lett.* **580**, 5880–5884.

Terstegen, L., Gatsios, P., Bode, J.G., Schaper, F., Heinrich, P.C. & Graeve, L. (2000) The inhibition of interleukin-6-dependent STAT activation by mitogen-activated protein kinases depends on tyrosine 759 in the cytoplasmic tail of glycoprotein 130. *J. Biol. Chem.* **275**, 18810–18817.

Tiganis, T., Kemp, B.E. & Tonks, N.K. (1999) The protein-tyrosine phosphatase TCPTP regulates epidermal growth factor receptor-mediated and phosphatidylinositol 3-kinase-dependent signaling. *J. Biol. Chem.* **274**, 27768–27775.

Tonks, N.K., Meng, T.C., Buckley, D.A., Galic, S. & Tiganis, T. (2004) Regulation of insulin signaling through reversible oxidation of the protein-tyrosine phosphatases TC45 and PTP1B. *J. Biol. Chem.* **279**, 37716–37725.

Wang, R., Cherukuri, P. & Luo, J. (2005) Activation of Stat3 sequence-specific DNA binding and transcription by p300/CREB-binding protein-mediated acetylation. *J. Biol. Chem.* **280**, 11528–11534.

Wen, Z. & Darnell, J.E. (1997) Mapping of Stat3 serine phosphorylation to a single residue (727) and evidence that serine phosphorylation has no influence on DNA binding of Stat1 and Stat3. *Nucleic Acids Res.* **25**, 2062–2067.

Wen, Z., Zhong, Z. & Darnell, J.E. (1995) Maximal activation of transcription by Stat1 and Stat3 requires both tyrosine and serine phosphorylation. *Cell* **82**, 241–250.

Wierenga, A.T., Vogelzang, I., Eggen, B.J. & Vellenga, E. (2003) Erythropoietin-induced serine 727 phosphorylation of STAT3 in erythroid cells is mediated by a MEK-, ERK-, and MSK1-dependent pathway. *Exp. Hematol.* **31**, 398–405.

Yamamoto, T., Sekine, Y., Kashima, K., Kubota, A., Sato, N., Aoki, N. & Matsuda, T. (2002) The nuclear isoform of protein-tyrosine phosphatase TC-PTP regulates interleukin-6-mediated signaling pathway through STAT3 dephosphorylation. *Biochem. Biophys. Res. Commun.* **297**, 811–817.

Yang, J., Huang, J., Dasgupta, M., *et al.* (2010) Reversible methylation of promoter-bound STAT3 by histone-modifying enzymes. *Proc. Natl Acad. Sci. USA* **107**, 21499–21504.

Yokogami, K., Wakisaka, S., Avruch, J. & Reeves, S.A. (2000) Serine phosphorylation and maximal activation of STAT3 during CNTF signaling is mediated by the rapamycin target mTOR. *Curr. Biol.* **10**, 47–50.

Yoshimura, A., Naka, T. & Kubo, M. (2007) SOCS proteins, cytokine signaling and immune regulation. *Nat. Rev. Immunol.* **7**, 453–465.

Yuan, Z.-L., Guan, Y.-J., Chatterjee, D. & Chin, Y.E. (2005) Stat3 dimerization regulated by reversible acetylation of a single lysine residue. *Science* **307**, 269–273.

Zhang, X., Guo, A., Yu, J., Possemato, A., Chen, Y., Zheng, W., Polakiewicz, R.D., Kinzler, K.W., Vogelstein, B., Velculescu, V.E. & Wang, Z.J. (2007) Identification of STAT3 as a substrate of receptor protein tyrosine phosphatase T. *Proc. Natl Acad. Sci. USA* **104**, 4060–4064.

Zhao, H., Nakajima, R., Kunimoto, H., Sasaki, T., Kojima, H. & Nakajima, K. (2004) Region 752-761 of STAT3 is critical for SRC-1 recruitment and Ser727 phosphorylation. *Biochem. Biophys. Res. Commun.* **325**, 541–548.

Received: 22 September 2011
Accepted: 9 November 2011

Supporting Information/supplementary material

The following Supporting Information can be found in the online version of the article:

Figure S1 No apparent effect of MG132 on the levels of STAT3 or phospho-Y705 levels.

Additional Supporting Information may be found in the online version of this article.

Please note: Wiley-Blackwell are not responsible for the content or functionality of any supporting materials supplied by the authors. Any queries (other than missing material) should be directed to the corresponding author for the article.

© 2012 The Authors
Journal compilation © 2012 by the Molecular Biology Society of Japan/Blackwell Publishing Ltd.

Journal of Child Neurology
000(00) 1-4
© The Author(s) 2011
Reprints and permission:
sagepub.com/journalsPermissions.nav
DOI: 10.1177/0883073811416239
http://jcn.sagepub.com
SAGE

Congenital Dysplastic Microcephaly and Hypoplasia of the Brainstem and Cerebellum With Diffuse Intracranial Calcification

Kazuyuki Nakamura, MD, Mitsuhiro Kato, MD, PhD, Ayako Sasaki, MD, PhD, Masayo Kanai, MD, PhD, and Kiyoshi Hayasaka, MD, PhD

Abstract

Congenital microcephaly with intracranial calcification is a rare condition presented in heterogeneous diseases. Here, we report the case of a 1-year-old boy with severe congenital microcephaly and diffuse calcification. Neuroimaging studies showed a diffuse simplified gyral pattern; a very thin cortex; ventricular dilatation; very small basal ganglia, thalamus, and brainstem; and cerebellar hypoplasia with diffuse calcification. Clinical features of intrauterine infections, such as neonatal jaundice, hepatomegaly, and thrombocytopenia, were not found. Serological tests, cultures, and polymerase chain reaction analysis were negative for viral infections. The etiology of pseudo–toxoplasmosis, rubella, cytomegalovirus, and herpes simplex syndrome is still unknown. This study describes the most severe form of pseudo–toxoplasmosis, rubella, cytomegalovirus, and herpes simplex syndrome reported to date, with the patient showing microcephaly and calcification or band-like intracranial calcification with simplified gyration and polymirogyria.

Keywords

microcephaly, intracranial calcification, pontocerebellar hypoplasia, toxoplasmosis, rubella, cytomegalovirus, herpes simplex

Received February 23, 2011. Accepted for publication June 16, 2011.

Congenital microcephaly with brain dysgenesis and intracranial calcification is a characteristic feature of intrauterine infections of toxoplasma, rubella, cytomegalovirus, herpes virus, and other infectious agents, including human immunodeficiency virus and the bacteria that cause syphilis. This form of congenital microcephaly has been termed the toxoplasmosis, rubella, cytomegalovirus, and herpes simplex syndrome.[1] In addition to congenital microcephaly and intracranial calcification, toxoplasmosis, rubella, cytomegalovirus, and herpes simplex syndrome shows systemic abnormalities, such as thrombocytopenia, anemia, hepatosplenomegaly, liver dysfunction, jaundice, and chorioretinitis, with elevated serum immunoglobulin M (IgM) levels at birth. Similar clinical conditions have been reported in several patients with familial occurrence but with no evidence of infection. These clinical conditions have been designated as "pseudo–toxoplasmosis, rubella, cytomegalovirus, and herpes simplex" syndrome.[2] In addition, "band-like intracranial calcification with simplified gyration and polymicrogyria" has also been reported. However, this syndrome shows no evidence of infection, abnormalities in liver function, or thrombocytopenia.[3,4]

It is important to discriminate these syndromes for genetic counseling. This report describes a patient with congenital microcephaly and whole brain dysgenesis and extensive calcification, suggesting a severe form of pseudo–toxoplasmosis, rubella, cytomegalovirus, and herpes simplex syndrome, or band-like intracranial calcification with simplified gyration and polymicrogyria.

Case Report

The boy was born to healthy, unrelated, 29-year-old Japanese parents. This was the mother's first pregnancy, and the boy had no siblings. There were no household pets including cats. During the 5- to 6-week period of gestation, his mother had fever for 1 day but showed no other symptoms. Microcephaly was first observed on ultrasound examination conducted at 28 weeks of gestation. At 34 weeks of gestation, specific IgMs

Department of Pediatrics, Yamagata University Faculty of Medicine, Yamagata, Japan

Corresponding Author:
Kazuyuki Nakamura, MD, Department of Pediatrics, Yamagata University Faculty of Medicine, 2-2-2, Iida-Nishi, Yamagata 990-9585, Japan
Email: kazun-yamagata@umin.ac.jp

Downloaded from jcn.sagepub.com at Tottori University on September 22, 2011

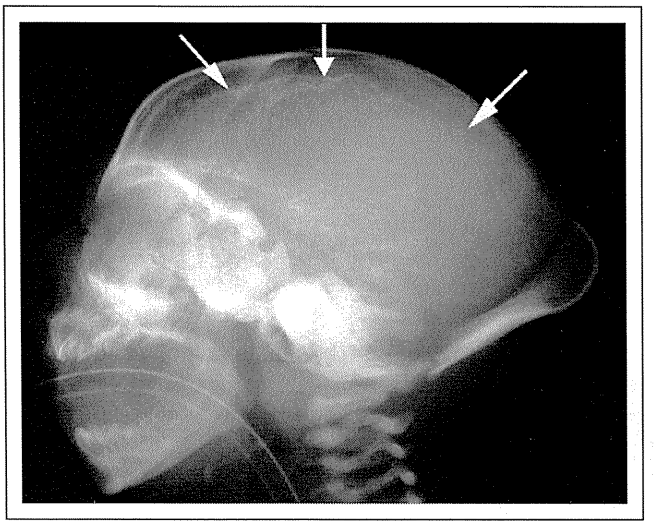

Figure 1. A plain radiograph of the head shows the cranial vault with a frontal sloping and a marked external occipital protuberance. Intracranial high-density spots are visible along the cerebral wall (arrows).

against rubella, cytomegalovirus, and toxoplasma were negative in the mother. He was delivered by caesarean section because of hypotonic uterine dysfunction at 42 weeks of gestation. His Apgar score was 1 at 1 min. He required intratracheal intubation for severe dyspnea. His weight at birth was 3140 g; length, 46 cm (−2.0 SD); and head circumference, 29 cm (−3.2 SD). He had bilateral undescended testis without hepatosplenomegaly or a petechial rash. Ophthalmologic examination showed no corneal clouding or chorioretinitis. Neurological examination showed the presence of hypotonic muscles and absence of a Moro reflex. Skull radiography showed a sloping forehead and several intracranial calcific densities (Fig. 1). A computed tomographic (CT) scan of the head showed prominent calcification mainly along the ventricular wall from the cerebrum to the brain stem (Fig. 2). Magnetic resonance imaging (MRI) of the brain showed severe diffuse simplified gyri combined with a thinning of the cortex and the white matter; marked dilated ventricles; and severe hypoplasia of the basal ganglia, thalamus, cerebellum, and brainstem (Fig. 3). At the age of 4 days, a hematological examination (hemoglobin, 18.3 g/dL; white blood cells, 10 010/μL; neutrophils, 69%; platelets, 32.8 $\times 10^4/\mu L^3$) and blood chemistry tests, including those for calcium, phosphate, aspartate aminotransferase, alanine aminotransferase, lactate, and amino acids were normal. The total serum IgM was 8 mg/dL; the specific IgMs against toxoplasma, rubella, cytomegalovirus, herpes simplex, and varicella-zoster virus were negative. Viral cultures of a pharyngeal swab and urine were negative. Subsequent polymerase chain reaction (PCR) amplification of cytomegalovirus DNA in urine and the umbilical cord was also negative. An antibody titer for lymphocytic choriomeningitis virus was negative. G-banding chromosomal analysis showed a karyotype of 46, XY. At the age of 10 months, a cerebrospinal fluid examination did not show increased number of lymphocytes or interferon-alpha.

Figure 2. Computed tomographic scan of the head shows linear or patchy high signals consisting of calcifications within or immediately beneath the cortex and the enlargement of the lateral ventricles.

Electroencephalography showed multifocal sharp waves with low-voltage background activity. At 12 months of age, he showed hypothermia (<36°C); recurrent urinary tract infections caused by vesicoureteral reflux; and a profound developmental delay with limb contractures, no eye contact, and no head control. He received tube feeding because of bulbar palsy.

Discussion

Congenital microcephaly results from various clinical conditions such as infections, radiation, exogenous toxic agents, anoxic or metabolic insults, and genetic bases.[1] Although these conditions can also cause cerebral calcification, the association of congenital microcephaly and calcification are rare. Our patient experienced a febrile episode, suggesting an infection at 5 to 6 weeks of gestation, but there was no history of any other insult. Since intrauterine infections or toxoplasmosis, rubella, cytomegalovirus, and herpes simplex syndrome, especially cytomegalovirus infection, is the most frequent cause of congenital microcephaly and since calcification and earlier infection induce severer brain anomalies,[1] we tried to obtain evidence of a prenatal infection of cytomegalovirus using serological tests, cultures, and PCR amplification. However, none of these tests yielded a positive result, which could be a result of early infection during fetal development. The fetus showed no immunological response, and the virus could not be cultured. Moreover, the PCR sensitivity was sufficiently high enough to detect viral DNA.[5] On

Downloaded from jcn.sagepub.com at Tottori University on September 22, 2011

Figure 3. Sagittal T2-weighted magnetic resonance imaging (MRI) shows a thin cortex and white matter with an undetectable border. Prominent hypoplasia of the cerebellum and brainstem is visible.

the basis of these results, we conclude that cytomegalovirus is unlikely to be the cause of our patient's condition.

During the middle embryonic period (5–6 weeks of gestation in humans), secondary brain vesicles (telencephalon, diencephalon, mesencephalon, metencephalon, and myelencephalon) are formed; the primitive cerebral hemispheres develop during neuronogenesis in the ventricular zone. Insult at this stage can engender extremely severe brain malformation (eg, decreased brain size) because of the inhibition of cell proliferation and the dysplastic configuration of the brain that results from impaired cell migration. The hypoplastic brainstem and cerebellum as well as microcephaly with the thin cortex and irregular convolution seen in our patient suggest an event during early embryogenesis, although the etiology is unknown.

Although our patient showed an irregular convolution that suggested possible cortical dysplasia, the very thin cortex suggested microcephaly with normal to thin cortex or microcephaly with a simplified gyral pattern.[6] To date, 5 genes (*MCPH1, ASPM, CDK5RAP2, CENPJ,* and *SLC25A19*) have been found to be responsible for the autosomal recessive inheritance of microcephaly with a simplified gyral pattern.[7,8] Mutations in these genes result in congenital microcephaly but not in a calcification resembling the one in our patient. Microcephaly with polymicrogyria or other cortical dysplasias or microcephaly with pontocerebellar hypoplasia are other candidate conditions for our patient, but neither one shows calcification.[9] At this point, it is difficult to categorize the neuroimaging features of our patient into the classification scheme for malformations of cortical development.[6]

Aicardi–Goutières syndrome is an autosomal recessive form of progressive encephalopathy characterized by acquired microcephaly, leukodystrophy, and calcifications of the basal ganglia, which is similar to toxoplasmosis, rubella, cytomegalovirus, and herpes simplex syndrome.[10] Recently, 5 genes (*TREX1, RNASEH2B, RNASEH2C, RNASEH2A,* and *SAMHD1*) have been identified as the responsible genes for this syndrome.[11-13] Elevated interferon-alpha levels and chronic lymphocytosis in the cerebrospinal fluid are specific features of Aicardi–Goutières syndrome. However, our patient had neither of these features. Although cerebrospinal fluid lymphocytosis is not necessary for an Aicardi–Goutières syndrome diagnosis[14] and although a small number of patients show microcephaly at birth, the cerebral dysplasia observed in our patient has never been reported as a manifestation of Aicardi–Goutières syndrome.

It has been suggested that pseudo–toxoplasmosis, rubella, cytomegalovirus, and herpes simplex syndrome is the same disorder as Aicardi–Goutières syndrome.[15] Periventricular areas are commonly calcified in pseudo–toxoplasmosis, rubella, cytomegalovirus, and herpes simplex syndrome, but the basal ganglia, cerebellum, and brainstem can also be affected. Brain MRIs often show cerebral atrophy, enlarged lateral ventricles, and severe hypoplasia of the corpus callosum, cerebellum, and brainstem. Some patients also show associated cortical dysplasia.[2,16] One report described a patient as having microcephaly with plate-like cortical calcification and with an extremely decreased convolution of the cerebral cortex, which is similar to our patient's condition.[17] However, the brainstem and cerebellum were spared in that patient.

Band-like intracranial calcification with simplified gyration and polymicrogyria is inherited as an autosomal recessive trait, and mutations of the *OCLN* gene have been identified as resulting in this condition.[18] Band-like intracranial calcification with simplified gyration and polymicrogyria is similar to pseudo–toxoplasmosis, rubella, cytomegalovirus, and herpes simplex syndrome in that both show widespread intracranial calcification and polymicrogyria and that some patients show hypoplasia of the cerebellum and brainstem. There are differences between these 2 conditions in terms of the postnatal microcephaly, the characteristic band-like calcification, and the lack of evidence for neonatal disturbance of liver function with thrombocytopenia; nonetheless, they can have similar etiologies.[3,4]

The extensive lesions of the brain are reminiscent of multicystic encephalomalacia, which are often accompanied by extensive dystrophic calcifications in zones of infarction. Multicystic encephalomalacia is also caused by fetal viral infection as well as hypoxia or circulatory insults; however, the lesions in the patient appeared to be too broad for secondary injury and had no visible cysts, as observed by MRI. The size and number of cysts depends on the stage of infarction, which can be both of major cerebral vessels and of the microcirculation at capillary levels.[19] Neuropathological confirmation is essential to reveal the pathogenesis.

It is noteworthy that this is the most severe case of a patient with congenital dysplastic microcephaly and brainstem and cerebellar hypoplasia with extensive intracranial calcification. The pathogenesis, particularly regarding its inheritance, remains to be clarified.

Acknowledgments

The authors thank Dr William B. Dobyns of the University of Chicago for his valuable comments and Dr Keiko Ishii, Tohoku University, for examining cytomegalovirus infection.

Downloaded from jcn.sagepub.com at Tottori University on September 22, 2011

Author Contributions

KN contributed in organizing the article and wrote the first draft of the manuscript. M. Kato and KH performed a review and critique of the manuscript. KN, M. Kato, AS, and M. Kanai primarily managed the patient.

Declaration of Conflicting Interests

The authors declared no potential conflicts of interest with respect to the research, authorship, and/or publication of this article.

Funding

The authors received no financial support for the research, authorship, and/or publication of this article.

Ethical Approval

The authors received an informed consent form from the parents of the patient.

References

1. Volpe JJ. In: *Neurology of the Newborn*. 5th ed. Philadelphia, PA: WB Saunders;; 2008.
2. Vivarelli R, Grosso S, Cioni M, et al. Pseudo-TORCH syndrome or Baraitser-Reardon syndrome: diagnostic criteria. *Brain Dev*. 2001;23:18-23.
3. Briggs TA, Wolf NI, D'Arrigo S, et al. Band-like intracranial calcification with simplified gyration and polymicrogyria: a distinct "pseudo-TORCH" phenotype. *Am J Med Genet A*. 2008;146: 3173-3180.
4. Abdel-Salam GM, Zaki MS, Saleem SN, Gaber KR. Microcephaly, malformation of brain development and intracranial calcification in sibs: pseudo-TORCH or a new syndrome. *Am J Med Genet A*. 2008;146:2929-2936.
5. Revello MG, Zavattoni M, Furione M, et al. Diagnosis and outcome of preconceptional and periconceptional primary human cytomegalovirus infections. *J Infect Dis*. 2002;186:553-557.
6. Barkovich AJ, Kuzniecky RI, Jackson GD, et al. A development and genetic classification for malformations of cortical development. *Neurology*. 2005;65:1873-1887.
7. Rosenberg MJ, Agarwala R, Bouffard G, et al. Mutant deoxynucleotide carrier is associated with congenital microcephaly. *Nat Genet*. 2002;32:175-179.
8. Woods CG, Bond J, Enard W. Autosomal recessive primary microcephaly (MCPH): a review of clinical, molecular, evolutionary findings. *Am J Hum Genet*. 2005;76:717-728.
9. Hashimoto K, Takeuchi Y, Kida Y, et al. Three siblings of fatal infantile encephalopathy with olivopontocerebellar hypoplasia and microcephaly. *Brain Dev*. 1998;20:169-174.
10. Goutières F. Aicardi-Goutières syndrome. *Brain Dev*. 2005;27: 201-206.
11. Crow YJ, Leitch A, Hayward BE, et al. Mutations in genes encoding ribonuclease H2 subunits cause Aicardi-Goutières syndrome and mimic congenital viral brain infection. *Nat Genet*. 2006;38: 910-916.
12. Crow YJ, Hayward BE, Parmar R, et al. Mutations in the gene encoding the 3'-5' DNA exonuclease TREX1 cause Aicardi–Goutières syndrome at the AGS1 locus. *Nat Genet*. 2006;38: 917-920.
13. Rice GL, Bond J, Asipu A, et al. Mutations involved in Aicardi–Goutières syndrome implicate SAMHD1 as regulator of the innate immune response. *Nat Genet*. 2009;41:829-832.
14. Crow YJ, Black DN, Ali M, et al. Cree encephalitis is allelic with Aicardi-Goutières syndrome: implications for the pathogenesis of disorders of interferon alpha metabolism. *J Med Genet*. 2003;40: 183-187.
15. Sanchis A, Cerveró L, Bataller A, et al. Genetic syndromes mimic congenital infections. *J Pediatr*. 2005;146:701-705.
16. Burn J, Wickramasinghe HT, Harding B, Baraitser M. A syndrome with intracranial calcification and microcephaly in two sibs, resembling intrauterine infection. *Clin Genet*. 1986; 30:112-116.
17. Kalyanasundaram S, Dutta S, Narang A, Katariya S. Microcephaly with plate-like cortical calcification. *Brain Dev*. 2003;25: 130-132.
18. O'Driscoll MC, Daly SB, Urquhart JE, et al. Recessive mutations in the gene encoding the tight junction protein occludin cause band-like calcification with simplified gyration and polymicrogyria. *Am J Hum Genet*. 2010;87:354-364.
19. Weiss JL, Cleary-Goldman J, Tanji K, et al. Multicystic encephalomalacia after first-trimester intrauterine fetal death in monochorionic twins. *Am J Obstet Gynecl*. 2004;190: 563-565.

Downloaded from jcn.sagepub.com at Tottori University on September 22, 2011

Pediatrics International (2012) ••, ••–••

doi: 10.1111/j.1442-200X.2011.03550.x

Patient Report

Hand-foot-genital syndrome with a 7p15 deletion: Clinically recognizable syndrome

Kana Hosoki,[1] Tohru Ohta,[2] Keinosuke Fujita,[3] Satsuki Nishigaki,[3] Masashi Shiomi,[4] Norio Niikawa[2] and Shinji Saitoh[1,5]

[1]*Department of Pediatrics, Hokkaido University Graduate School of Medicine, Sapporo,* [2]*Research Institute of Personalized Health Sciences, Health Science University of Hokkaido, Tobetsu, Departments of* [3]*Pediatrics and* [4]*Pediatric Emergency Medicine, Osaka City General Hospital, Osaka and* [5]*Department of Pediatrics and Neonatology, Nagoya City University School of Medical Sciences, Nagoya, Japan*

Key words developmental delay, hand-foot-genital syndrome, *HOXA* cluster, *HOXA13*, 7p15 deletion.

Hand-foot-genital syndrome (HFGS; MIM 140000) is a congenital limb malformation syndrome involving small hands and feet with unusually short great toes and abnormal thumbs.[1] HFGS is caused by mutations in *HOXA13* located on 7p15.2, a *HOXA* family member that correlates to construct patterning of the vertebrate.[2] Patients with a deletion encompassing *HOXA13* also have typical features of HFGS.[3]

Many deletions involving 7p15 have been reported. All deletions involving *HOXA13* include HFGS features.[3–6] Nevertheless, because larger deletions often show severe clinical features, HFGS phenotypes may not be recognized in such large-deletion cases. In contrast, patients with smaller deletions involving 7p15 appear to have mild developmental delay and characteristic facies in association with HFGS.[5,6]

Here we report on a patient with a 6.9 Mb deletion at 7p15. Compared to previous studies, we propose that a small deletion of 7p15 causes a clinically recognizable syndrome.

Case report

Patient

The boy was born at 39 weeks of gestation as the fourth child of healthy parents. Other family members were also healthy. His birthweight, length, and head circumference were 2560 g (–1.2 SD), 48.0 cm (–0.5 SD), and 32.5 cm (–0.2 SD), respectively. In the neonatal period he developed feeding difficulty. He showed mild developmental delay, and acquired head control at age 3 months, rolling over at 7 months, unassisted walk at 14 months, and meaningful words at 15 months.

At age 10 years he was suspected of having Prader–Willi syndrome (PWS) for his small hands and feet, short stature, developmental delay, feeding difficulty during infancy and mild obesity, which developed after childhood. Examination at 13 years showed a height of 138 cm (–2.5 SD), and a weight of 44 kg (–0.5 SD). He exhibited mildly dysmorphic facies including bifrontal narrowing and low-set posterior rotated dysplastic ears (Fig. 1a,d). He did not have ophthalmological or audiological complications. He had small hands and feet with clinodactyly of the bilateral fifth finger, and short, curved and broad great toes (Fig. 1b,e,g). X-ray demonstrated small pointed distal phalanges and hypoplastic middle phalange of the fifth digits (Fig. 1c), and hypoplasia of the middle and distal phalanges (Fig. 1f). Bone age at 10 years 4 months was delayed and estimated to be 6 years 6 months. Genital anomaly was not present. He did not have intellectual or behavioral problems and attended regular primary school although a formal IQ test has not been done.

Prader–Willi syndrome and maternal uniparental disomy 14 (upd(14)mat) syndrome was excluded on genetic tests (data not shown),[7] and G-band chromosomal analysis showed a normal karyotype of 46,XY. Microarray analysis was then performed, as described in the following section.

DNA methylation analysis

Genomic DNA was isolated from peripheral blood leukocytes of the patient and his parents. DNA-methylation-specific polymerase chain reaction for *SNRPN* at 15q11.2 and *MEG3* at 14q32.2 was performed as described previously to rule out PWS and upd(14)mat syndromes.[7]

Microarray analysis

We performed a chromosomal microarray analysis using Genome-Wide Human SNP Nsp/Sty Array Kit 5.0 (Affymetrix, Santa Clara, CA, USA) for genomic DNA isolated from peripheral blood leukocytes of the patient and his parents. Microarray analysis of the patient detected a 6.9 Mb deletion at 7p15.3-p15.1 [arr7p15.3p15.1(22 460 185–29 360 960)x1] (Fig. 2). This deletion was not identified in his parents, indicating the de novo origin of the deletion. Single nucleotide polymorphism (SNP) genotyping in the deleted region showed that the deletion was of

Correspondence: Shinji Saitoh, MD PhD, Department of Pediatrics and Neonatology, Nagoya City University School of Medical Sciences, Kawasumi 1, Mizuho-cho, Mizuho-ku, Nagoya 467-8601, Japan. Email: ss11@med.nagoya-cu.ac.jp

Received 28 June 2011; revised 24 October 2011; accepted 9 November 2011.

© 2012 The Authors
Pediatrics International © 2012 Japan Pediatric Society

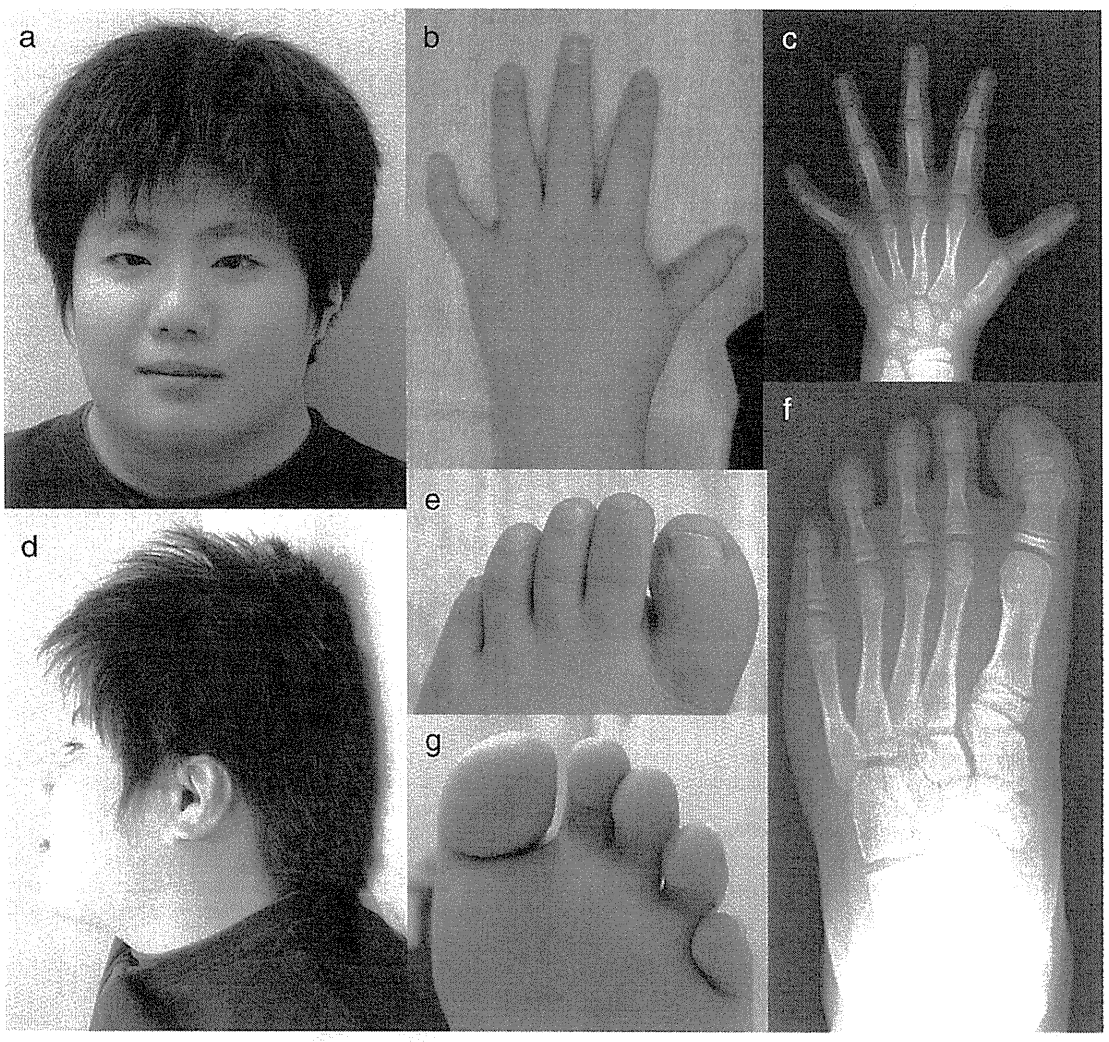

Fig. 1 Facial expression and limb abnormalities in the present patient. (a) Mildly dysmorphic facies with bifrontal narrowing. (d) Lateral view demonstrating low-set posterior rotated dysplastic ears. (b) Left hand showing short digits and clinodactyly of the fifth finger. (c) X-ray showing small pointed distal phalanges and hypoplasia of the middle phalange of the fifth digit. (e,g) Left foot showing a short, curved and broad great toe. (f) X-ray showing hypoplasia of the middle and distal phalanges.

paternal origin (data not shown). The deletion contained the *HOXA* cluster including *HOXA13* as well as 56 other genes (Fig. 2).

Discussion

Hand-foot-genital syndrome caused by a deletion encompassing *HOXA13* shows additional features, such as mildly dysmorphic facies, developmental delay, feeding difficulty in the neonatal period, and borderline mentality or intellectual disability.[3,5,6] Four patients with a small deletion involving *HOXA13* located at 7p15 have been reported.[3,5,6] The present patient, with manifestations similar to those of the four previous cases, had a deletion containing *HOXA13*. This let us make further delineation of HFGS, that is, 'deletion-positive' (deletion+) HFGS (Table 1). Although the ear, nose and eye of the five patients with deletion+ HFGS were mildly dysmorphic, their facial characteristics remained inconclusive. Developmental delay, albeit mild, was present in all five patients, and intelligence varied from normal to mildly disabled. It is noteworthy that three of the five patients had neonatal feeding difficulty. Deletion+ HFGS may involve developmental

© 2012 The Authors
Pediatrics International © 2012 Japan Pediatric Society

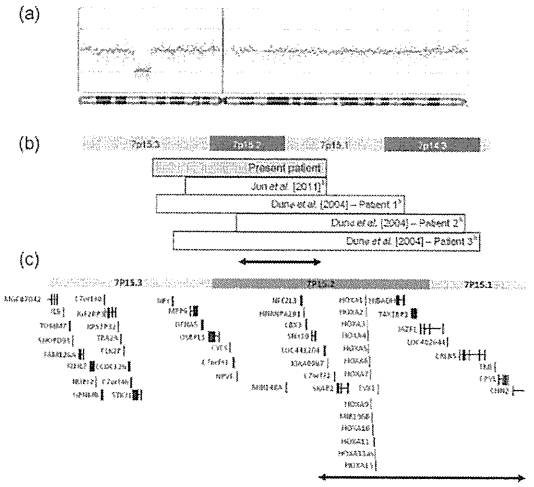

Fig. 2 Microarray results of the patient. (a) 6.9 Mb interstitial deletion at 7p15.3-p15.1 [arr7p15.3p15.1(22 460 185–29 360 960)x1]. (b) Overlapping deletions of five patients.[5,6] Shortest region of overlap (SRO; arrow) is approximately 2 Mb. (c) Schematic of included genes in the deletion region. Genome coordinates are according to the 36.1 build (March 2006) of the human reference genome at the UCSC database (http://genome.ucsc.edu/). The SRO (arrow) is defined from the proximal border of the deletion of Dunø *et al.*'s patient 2 to the distal border of that of the present patient (chr7:26 374 754–29 360 960), containing nine genes plus *HOXA* cluster.[5] In addition, the Dunø *et al.* reported positions were arranged from the 34 build (July 2003) to 36.1 build.[5]

delay, feeding difficulty in the neonatal or infantile period and short stature in addition to small hands/feet and genital anomaly. Therefore, it is possible that the patients could be suspected to have PWS. This pattern of abnormalities might cause attending physicians to suspect PWS, as was the case for the present patient. Nevertheless, limb abnormalities of HFGS are distinct from those of PWS. Bone abnormalities frequently found in HFGS are not present in PWS. Therefore, detailed clinical investigation including X-ray examination of hands and feet may be of help to differentiate HFGS from PWS.

The 2.0 Mb shortest region of overlap (SRO) among the five patients with deletion+ HFGS is defined from the proximal border of the deletion of Dunø *et al.*'s patient 2 to the distal border of that of the present patient, and should define its critical region (Fig. 2).[5] The exact breakpoints of Jun *et al.*'s patient were not certain because the reference sequence was not provided, but the distal breakpoint should be similar to that of the present patient because it was located between *STK31* and *CHN2*.[6] Because the distal breakpoint of the present patient is located within 7p15.1, several genes located more distally are excluded from candidacy for deletion+ HFGS. The SRO among the five patients contains nine genes other than the *HOXA* cluster (Fig. 2). Among the nine genes, only *JAZF1* (*TIP27*) was designated as a morbid gene, according to the OMIM database (http://www.ncbi.nlm.nih.gov/omim/). *JAZF1* was initially identified as a 7p15-derived participant in the fusion gene resulting from t(7;17)(p15;q21) translocation in endometrial stromal sarcoma cells.[8] Genome-wide association study demonstrated that an SNP in *JAZF1* is associated with type 2 diabetes, but there have been

Table 1 Clinical features on five patients with 7p15 deletion

Age (years), sex	Patient 1 Present case 13, male	Patient 2 Jun *et al.* (2011)[6] 4, male	Patient 3 Dunø *et al.* (2004)[5] case 1 5, female	Patient 4 Dunø *et al.* (2004)[5] case 2 4, male	Patient 5 Dunø *et al.* (2004)[5] case 3 21, male
Chromosomal deletion					
Location	7p15.3p15.1	7p15.3p15.1	7p15.3p14.3	7p15.2p14.2	7p15.3p14.2
Size (Mb)	6.9	5.6	9.8	9.0	12
Inheritance (parental origin)	De novo (paternal)	De novo	De novo	De novo	De novo (maternal)
Development					
Developmental delay	+	+	+	+	NA
Speech delay	+	+	+	+	NA
Limb anomaly					
Small hands and feet	+	+	+	+	NA
Clinodactyly of fingers	5th both	–	4th right	5th both	5th both
Other finger anomaly	–	Limited extension (1st, 2nd, 3rd)	Short fingers	Short fingers	Thumb anomaly
Great toe anomaly	Curved and broad	Hypoplasia	Short and broad	NA	Hypoplasia
Other toe anomaly	Short toes	NA	NA	Short toes pes planus	NA
Genital anomaly					
Genital abnormality	–	Hypospadias	NA	NA	Cryptorchidism
Facial features					
Low-set ears	+	+	NA	NA	+
Ear anomaly	Posterior rotated	Posterior angulated	NA	Short, slightly deformed	NA
Palpebral fissures anomaly	–	Upslanted	Upslanted	Downslanted	Upslanted
Flat nasal bridge	–	+	+	NA	NA
Nostril anomaly	–	NA	Anteverted	NA	Upturned
Forehead anomaly	Bifrontal narrowing	Frontal bossing	NA	NA	NA
Other facial anomaly	–	NA	Broad lips broad nose	Broad neck	Large mouth retrognathia
Other features					
Short stature	+	+	NA	+	NA
Neonatal feeding difficulty	+	+	NA	NA	+

+, feature present; –, feature absent; NA, not available.

© 2012 The Authors
Pediatrics International © 2012 Japan Pediatric Society

no data on the relationship between *JAZF1* and neurodevelopment or brain function.[9]

Nonetheless, it remains inconclusive as to which genes are responsible for additional phenotypes in deletion+ HFGS. Further collection of cases of deletion+ HFGS will facilitate identification of responsible genes.

Acknowledgments

We are deeply grateful to the patient and his family for participating in this study. We also thank Professor Tadashi Ariga for his thoughtful advice on this report.

References

1 Goodman FR. Limb malformations and the human *HOX* genes. *Am. J. Med. Genet. A* 2002; **112**: 256–65.
2 Mortlock DP, Innis JW. Mutation of *HOXA13* in hand-foot-genital syndrome. *Nat. Genet.* 1997; **15**: 179–80.
3 Devriendt K, Jaeken J, Matthijs G *et al.* Haploinsufficiency of the *HOXA* gene cluster, in a patient with hand-foot-genital syndrome, velopharyngeal insufficiency, and persistent patent ductus botalli. *Am. J. Hum. Genet.* 1999; **65**: 249–51.
4 Hoover-Fong JE, Cai J, Cargiles CB *et al.* Facial dysgenesis: A novel facial syndrome with chromosome 7 deletion p15.1–21.1. *Am. J. Med. Genet. A* 2003; **117**: 47–56.
5 Dunø M, Hove H, Kirchhoff M, Devriendt K, Schwartz M. Mapping genomic deletion down to the base: A quantitative copy number scanning approach used to characterise and clone the breakpoints of a recurrent 7p14.2p15.3 deletion. *Hum. Genet.* 2004; **115**: 459–67.
6 Jun KR, Seo EJ, Lee JO, Yoo HW, Park IS, Yoon HK. Molecular cytogenetic and clinical characterization of a patient with a 5.6-Mb deletion in 7p15 including *HOXA* cluster. *Am. J. Med. Genet. A* 2011; **155A**: 642–7.
7 Hosoki K, Kagami M, Tanaka T *et al.* Maternal uniparental disomy 14 syndrome demonstrates Prader-Willi syndrome-like phenotype. *J. Pediatr.* 2009; **155**: 900–3.
8 Koontz JI, Soreng AL, Nucci M *et al.* Frequent fusion of the JAZF1 and JJAZ1 genes in endometrial stromal tumors. *Proc. Natl Acad. Sci. USA* 2001; **98**: 6348–53.
9 Zeggini E, Scott LJ, Saxena R *et al.* Meta-analysis of genome-wide association data and large-scale replication identifies additional susceptibility loci for type 2 diabetes. *Nat. Genet.* 2008; **40**: 638–45.

© 2012 The Authors
Pediatrics International © 2012 Japan Pediatric Society

ELSEVIER

Brain & Development 34 (2012) 20–27

BRAIN & DEVELOPMENT
Official Journal of the Japanese Society of Child Neurology

www.elsevier.com/locate/braindev

Original article

Thermolabile CPT II variants and low blood ATP levels are closely related to severity of acute encephalopathy in Japanese children

Masaya Kubota [a,b], Junji Chida [c], Hideki Hoshino [a], Hiroshi Ozawa [b], Ayaka Koide [b], Hirohumi Kashii [a,b], Akiko Koyama [a], Yoko Mizuno [b], Ai Hoshino [b], Miyoko Yamaguchi [c], Dengbing Yao [c], Min Yao [c], Hiroshi Kido [c,*]

[a] *Division of Neurology, National Center for Child Health and Development, 2-10-1 Ohkura, Setagaya-Ku, Tokyo, Japan*
[b] *Department of Pediatrics, Metropolitan Hachioji Children's Hospital, Tokyo, Japan*
[c] *Division of Enzyme Chemistry, Institute for Enzyme Research, The University of Tokushima, Kuramoto-cho 3-18-15, Tokushima 770-8503, Japan*

Received 5 May 2010; received in revised form 10 October 2010; accepted 27 December 2010

Abstract

Despite the decrease in Reye syndrome after the discontinuation of aspirin, acute encephalopathy (non-Reye syndrome type) has been continually reported in Japan. Recent studies suggested that the thermolabile phenotype of carnitine palmitoyltransferase II (CPT II) variation [F352C] was closely related to the pathomechanism of influenza-associated encephalopathy (IAE) in Japanese, causing mitochondrial ATP utilization failure during periods of high fever, resulting in brain edema. So, we analyzed CPT II polymorphism and peripheral blood ATP levels as a signal of "energy crisis" in 12 and 10 patients with acute encephalopathy, respectively. Out of the 12 patients with acute encephalopathy, six showed thermolabile CPT II variants [F352C], and of these six, two patients died in spite of intensive care. In contrast, the remaining six patients with no thermolabile CPT II variant [F352C] showed a relatively mild clinical course. Blood ATP levels of the 10 patients in the acute phase of encephalopathy were significantly lower than those during the convalescent phase and also those of patients with febrile seizure status. Our data suggest that the thermolabile F352C CPT II variant, found only in Japanese, might be one of the predisposing factors to trigger the pathomechanism of acute encephalopathy in the Japanese population, and that it is causally related to the severity of disease. The decreased blood ATP level seems to reflect systemic mitochondrial dysfunction including the blood brain barrier during the acute phase of encephalopathy.
© 2011 The Japanese Society of Child Neurology. Published by Elsevier B.V. All rights reserved.

Keywords: Acute encephalopathy, Carnitine palmitoyltransferase II; Thermolabile variants; ATP; Mitochondrial dysfunction

1. Introduction

Acute encephalopathy in children is clinically characterized by high fever, prolonged consciousness disturbance associated with brain edema, and prolonged or multiple generalized seizures. Acute encephalopathy distinct from Reye syndrome is not rare in Japan. The precise pathogenesis of acute encephalopathy including influenza-associated encephalopathy (IAE) remains unclear. An epidemiological study revealed that aspirin use was closely related to the pathogenesis of Reye syndrome [1]. However, despite the decrease in Reye syndrome after the discontinuation of aspirin, acute encephalopathy (non-Reye syndrome type) has been continually reported in Japan [2].

Recently, acute encephalopathy was classified into several types according to magnetic resonance imaging (MRI) findings together with the clinical course, such

* Corresponding author. Tel.: +81 88 633 9649; fax: +81 88 633 7425.
E-mail address: kido@ier.tokushima-u.ac.jp (H. Kido).

0387-7604/$ - see front matter © 2011 The Japanese Society of Child Neurology. Published by Elsevier B.V. All rights reserved.
doi:10.1016/j.braindev.2010.12.012

as acute necrotizing encephalopathy [3], acute encephalopathy with biphasic seizures and late reduced diffusion [4], and hemorrhagic and shock encephalopathy [5,6]. Although the influenza virus and HHV-6 (human herpes virus-6) are the main causative agents of these acute encephalopathies, many other viruses are also considered to be responsible for the disease [3,4,7].

It is estimated that more than 100 children die of IAE every year in Japan [8,9]. According to the first nationwide clinical survey of IAE in Japan, in many patients with IAE, multiple-organ failure developed, and rates of mortality (31.8%) and disability (27.7%) were high [2]. Although clinical and neuropathological studies suggested that blood–brain barrier destruction and hypercytokinemia in cerebrospinal fluid were closely related to the pathogenesis of IAE, the pathophysiology and mechanisms of disease onset are still unclear [3,7,10,11].

Recently, Chen et al. [12] reported that the thermolabile phenotypes of carnitine palmitoyltransferase II (CPT II) variations, [1055T > G/F352C] alone, and [1055T > G/F352C] + [1102G > A/V368I] were closely related to the pathomechanisms of IAE. The CPT system is a pivotal component of ATP generation through mitochondrial fatty acid oxidation in mammals [13]. Yao et al. [14] further characterized the enzyme properties of the CPT II variants as follows: (1) dominant-negative effect, (2) reduced activities, (3) thermal instability, and (4) short half-lives compared with the wild-type. They demonstrated that the thermolabile CPT II variants might cause mitochondrial fuel utilization failure in various organs and endothelial cells during periods of high fever, and, thus, might play an important role in the pathogenesis of brain edema in IAE. In the present study, we analyzed the CPT II polymorphism and peripheral blood ATP levels as a signal of "energy crisis" in patients with acute encephalopathy with and without influenza virus infection, septic encephalopathy, and febrile delirium during influenza virus infection, and analyzed the relationships among these data, age, and clinical manifestations.

2. Patients and methods

2.1. Patient profile for the study of CPT II polymorphism

This investigation was approved by the Ethics Review Committee for human genome analysis of our institution. All participants' caregivers gave written informed consent. Fifteen patients were included in the study. The clinical details are summarized in Table 1. The diagnoses of the 15 patients were as follows: 12 patients with acute encephalopathy (7 IAE, one human herpes virus type 6 (HHV-6) associated, one varicella-associated, one septic encephalopathy associated with *Hemophilus influenzae* type b, two acute encephalopathy with an unknown pathogenesis, highly suspected of being of viral origin), and three febrile delirium associated with influenza virus infection. Two patients (Case 1, IAE, and Case 2, septic encephalopathy) died 30 and 3 days after admission, respectively, despite intensive care. All 12 patients with acute encephalopathy were diagnosed based on prolonged seizures with high fever and/or consciousness disturbance lasting longer than 12 h associated with brain CT or MRI abnormalities.

3. Representative case presentations

3.1. Case 1

This 4-year-old girl was admitted to our hospital because of feeding difficulty, a lethargic state, and high fever lasting longer than 12 h. A rapid test for influenza A virus antigen in the nasal discharge was positive. She has been followed at our outpatient clinic with a diagnosis of severe psychomotor delay and epilepsy due to chromosome abnormality (46, XX, dup(2)(q21.1q24.2)) since the age of 3 years. Her seizure disorder was well-controlled with phenobarbital. On admission, except for a lethargic tendency, she showed no neck stiffness, involuntary movement, or convulsion, and her respiratory and circulatory conditions were stable. She was also able to follow an object. Neurological examination revealed normal light and corneal reflexes and normal deep tendon reflexes. Pathological reflexes were not induced. Her consciousness level, however, deteriorated 12 h after admission. On laboratory tests, blood glucose, ammonia, the white blood cell count (WBC), hemoglobin (Hb), and platelet count (Plt) were within normal ranges, and cereblospinal fluid (CSF) findings were unremarkable. Blood and CSF cultures were negative. Because she also showed sudden respiratory insufficiency and reduced blood pressure, she was immediately resuscitated and intubated. After that, she could not move and all brainstem reflexes disappeared. On brain CT the next day, as shown in Fig. 1a, cisterns surrounding the brainstem and cerebellum were not identified and auditory brainstem responses (ABR) showed only bilateral wave I. Rapid consciousness deterioration as well as brain CT and ABR findings suggested cerebral herniation due to influenza-associated brainstem encephalopathy. On the second CT 3 weeks later, severe brain edema and subarachnoid hemorrhage were observed. Despite intensive care, she died on the 31st day of hospitalization. She had a thermolabile F352C CPT II variant.

3.2. Case 2

This previously healthy 2-year-old boy was admitted to our hospital because of consciousness disturbance, a brief seizure cluster, and high fever lasting 24 h. On admission, neurological examination revealed coma, the absence of light and corneal reflexes, dilated and anisocoric pupils, and flaccid extremities. Neck stiffness was

Table 1
Clinical summary of patients and CPT II polymorphism.

Case no.	Age at onset	Pathogen	Diagnosis	CPT II polymorphism	Duration of high fever	Duration of seizure (min)	Therapy	Outcome
1[c]	4 years 10 months	Flu A	IAE	F352C	24 h	(–)	Gly, IVIG, m-PSL, Venti	Died
2	2 years 2 months	*H. influenza*	Hib septic AE	F352C, V368I	2 days	3	Venti, Epin, DOA, CTX	Died
3[c]	1 year	Unknown	AEU	F352C, V368I	2 days	30	Mann, MDZ	Severe MR, MD, Epi
4[c]	1 year 7 months	Flu A	IAE	(–)	30 h	40	Gly, m-PSL, Venti	Moderate MR, MD, Epi
5[a]	4 years 5 months	Flu A	IAE	F352C, V368I	5 days	90	Gly, MDZ, Pen, IVIG, m-PSL	Moderate MR
6[a]	2 years 1 months	Varicella	Varicella AE	F352C, V368I	24 h	90	Mann, MDZ, m-PSL	Mild MR
7[c]	6 years	Unknown	AEU	F352C, V368I	2 days	30	Mann, MDZ, m-PSL, HT	Mild MR
8[a]	1 years 4 months	Flu A	IAE	V368I	5 days	60	Gly, MDZ, Pen, PB, m-PSL	Mild MR
9[a]	2 years	Flu A	IAE	V368I	5 days	60	Gly, MDZ, Pen, IVIG, m-PSL	Mild MR
10[a]	11 months	HHV-6	HHV-6 AE	V368I	36 h	100	Gly, MDZ, Pen, m-PSL	Good
11[b]	2 years 5 months	Flu A	IAE	V368I, M647 V	24 h	40	MDZ, PB, m-PSL, HT	Good
12[a]	3 years 11 months	Flu A	IAE	V368I	2 days	40	MDZ, PB, m-PSL, HT, Venti	Good
13	4 years 9 months	Flu A	FD	F352C, V368I	4 days	2	(–)	Good
14	9 years 5 months	Flu A	FD	(–)	3 days	(–)	(–)	Good
15	11 years	Flu A	FD	V368I, M647V	3 days	(–)	(–)	Good

IAE: Influenza-associated encephalopathy, AEU: acute encephalopathy of unknown pathogen, FD: febrile delirium, Flu A: influenza A, HHV-6: human herpes virus-6, MR; mental retardation, MD: motor delay, Epi: epilepsy, Mann: mannitol, MDZ: midazolam, m-PSL: methylpredonisolone, HT: hypothermia, Venti: artificial ventilator, Epin: epinephrine, DOA: dopamine, CTX: cefotaxim, PB: Phenobarbital, Pen: pentobarbital, IVIG: intravenous infusion of gamma-globlin, Gly: glycerole.

[a] AESD (acute encephalopathy with biphasic seizures and late reduced diffusion).

[b] This case partially resembles ANE (acute necrotizing encephalopathy).

[c] Unclassified acute encephalopathy.

not observed. A rapid test for influenza virus antigen in the nasal discharge was negative. His head CT demonstrated diffuse brain edema, as shown in Fig. 1b. On laboratory investigation, blood glucose and ammonia, as well as liver and renal functions were within normal limits. WBC was 18,000/μL, Hb 11.6 g/dL, Plt 3,60,000/μL, and prothrombin time 68.7 s. Blood culture identified *H. influenzae* type b. Spinal tap was not performed because of the risk of cerebral herniation. The blood ATP level was 0.58 mM on admission. The acylcarnitine ratio ((C16 + C18:1)/C2) was high, at 0.203, on admission, compared with the upper cutoff value of 0.048 [12]. We diagnosed him with septic encephalopathy. Despite intensive care including antibiotics, ventilator support, and catecholamine infusion, he died 2 days later. He had compound thermolabile CPT II variants [F352C + V368I].

3.3. Case 12

This previously healthy 3-year-old boy was admitted to our hospital because of a febrile seizure status and high fever lasting longer than 24 h. His generalized tonic clonic seizure was suppressed with pentobarbital infusion 40 min after the onset. A rapid test for influenza virus antigen in the nasal discharge was positive for flu A. Brain CT revealed mild brain edema. So, he was sedated and intubated. Methylpredonisolone (m-PSL) pulse and hypothermia therapies were immediately started based on the diagnosis of IAE. The blood ATP value was 0.77 mM on admission, and it increased to 1.35 mM 2 weeks later. On the 6th day of hospitalization, he developed brief right-sided clonic seizure. Brain MRI (diffusion-weighted images) showed an abnormal high intensity in the left hemisphere (Fig. 1e). The clinical course and MRI findings were compatible with acute encephalopathy with biphasic seizures and late reduced diffusion [4]. Additional m-PSL therapy was given and the hypothermia therapy gradually discontinued. His neurological condition subsequently showed a full recovery. No apparent mental, motor, and social skill impairment was noted during follow-up 1 year later. He had a V368I CPT II variant.